Time-Dependent Density Functional Theory (TDDFT) Study of the Excited Charge-Transfer State Formation of a Series of Aromatic Donor−Acceptor Systems

Christine Jamorski Jödicke* and Hans Peter Lüthi

Contribution from the Laboratorium für Physikalische Chemie, ETH Hoenggerberg, CH-8093 Zürich, Switzerland

Abstract: Singlet excitation energy calculations for a series of acceptor para-substituted *N*,*N*-dimethyl-anilines that are dual (4-(*N*,*N*-dimethylamino)benzonitrile, 4DMAB-CN, 4-(*N*,*N*-dimethylamino)benzaldhyde, 4DMAB-CHO, 1-methyl-7-cyano-2,3,4,5-tetrahydro-1*H*-1-benzazepine, NMC7) and nondual (4-aminoben-zonitrile, 4AB-CN, 3-(*N*,*N*-dimethylamino)benzonitrile, 3DMAB-CN, and 4-nitro(*N*,*N*-dimethyl) aniline, 4DMAB-NO$_2$) fluorescent have been performed using time-dependent density functional theory (TDDFT). The B3LYP and MPW1PW91 functionals with a 6-311+G(2d,p) (Bg) basis set have been used to compute excitation energies. Ground-state geometries were optimized using density functional theory (DFT) with both B3LYP and MPW1PW91 functionals combined with a 6-31G(d) basis set. For most of the molecules presented in this study, potential energy surfaces have been computed according to the coordinates related to the three following mechanisms proposed in the literature: twisting, wagging, and planar intramolecular charge transfer (ICT). Comparison of the three models for the different molecules leads to the conclusion that only the twisting ICT model is able to explain the low frequency, strongly solvent-dependent energy band present in the fluorescence spectra. According to this model, the 4AB-CN molecule is calculated to be nondual fluorescent in agreement with the experimental spectra. The single band observed in the fluorescence spectra of TMAB-CN (4-(*N*,*N*-dimethylamino)-3,5-(dimethyl)benzonitrile) is due to a large stabilization of the charge-transfer excited state along the twisting coordinate. The nondual fluorescence of the 4DMAB-NO$_2$ molecule is explained by the same mechanism. In the case of 3DMAB-CN, the single observed emission, which is solvent-dependent, has been assigned to the lowest charge-transfer excited state. The dual fluorescence of 4DMAB-CN and 4DMAB-CHO is explained within the twisting ICT model by a double mechanism (already proposed by Serrano et al.: Serrano-Andrés, L.; Merchán, M.; Roos, B. J.; Lindh, R. *J. Am. Chem. Soc.* **1995**, *117*, 3189) that involves the presence of two low-lying states close enough in energy. The observation of dual fluorescence in NMC7, that has been one of the origins of the planar ICT model put forward by Zachariasse et al. (Zachariasse, K.; van der Haar, T.; Hebecker, A.; Leinhos, U.; Kühnle, W. *Pure Appl. Chem.* **1993**, *65*, 1745), could be fully understood by a double mechanism within the twisting ICT model. Within the set of investigated molecules, our calculations confirm that the twisting ICT model is the only mechanism acceptable to explain the dual and nondual fluorescence phenomenon. Our calculations are in complete agreement with experimental data.

I. Introduction

For several years now, intense research in the field of nonlinear optical and electrooptical organic material triggered by their possible application as electrooptical switches, chemical sensors, and fluorescence probes has developed.[3−5] The presence of electron donor and acceptor groups on opposite sides of the molecule, connected by a highly delocalized π electron system, is key to their nonlinear optical properties. Recently, the dual fluorescence property of donor acceptor systems has been used in the context of molecular switches.[6]

The phenomenon of dual fluorescence, first discovered by Lippert et al.[7] 40 years ago in compounds such as 4-(*N*,*N*-dimethylamino)benzonitrile (4DMAB-CN), is an example of a more general process involving photoadiabatic reaction in the excited state. Since then, this feature has been observed in a

* To whom correspondence should be addressed. E-mail: christin@igc.phys.chem.ethz.ch.

(1) Serrano-Andres, L.; Merchan, M.; Roos, B. J.; Lindh, R. *J. Am. Chem. Soc.* **1995**, *117*, 3189.

(2) Zachariasse, K.; van der Haar, T.; Hebecker, A.; Leinhos, U.; Kiihnle, W. *Pure Appl. Chem.* **1993**, *65*, 1745.

(3) Bosshard, Ch.; Sutter, K.; Pretre, Ph.; Hulliger, J.; Florsheimer, M.; Kaatz, P.; Giinter, P. Organic Nonlinear Optical Materials. *Advances in Nonlinear Optics*; Gordon and Breach Publishers: Langhorne, PA, 1995; Vol. 1.

(4) Kippelen, B.; Lackritz, H. S.; Claus, R. O. *Organic Nonlinear Optical Material and Devices*; P.A. Materials Research Society, 1999.

(5) Lakowicz, J. P. *Principles of Fluorescence Spectroscopy*, 2nd ed.; Kluwer Academic: Hongham, 1999.

(6) (a) La Chair, J. J. *Angew. Chem., Int. Ed.* **1999**, *38*, 3047. (b) La Chair, J. J. *Angew. Chem., Int. Ed.* **1998**, *37*, 325. (c) La Chair, J. J. *Angew. Chem., Int. Ed.* **1998**, *110*, 339. (d) La Chair, J. J. *J. Am. Chem. Soc.* **1997**, *119*, 7676.

(7) (a) Lippert, E.; Lippert, W.; Moll, F.; Nagele, W.; Boos, H.; Prigge, H.; Seibold-Blankenstein, I. *Angew. Chem.* **1961**, *73*, 695. (b) Lippert, E.; Liider, W.; Boss, H. *Advances in Molecular Spectroscopy*; 1962; p 443.

large variety of compounds such as nonsubstituted linear polyenes as well as in donor−acceptor systems, structurally similar to 4DMAB-CN.[2,8−18]

The fluorescence spectrum of 4DMAB-CN consists of the so-called normal band, L_b, which shows a short-axis polarization at the blue edge of the spectrum and a long-axis polarization for the rest of the band. The abnormal band, L_a, which exhibits only long-axis polarization is observed at lower energy. In polar solvents, the L_a emission, which is strongly red shifted, has been explained by the existence of an intramolecular charge-transfer state with a large dipole moment. On the other hand, the nondependence on the polarization of the media of the L_b band is explained by an emission arising from the less polar locally excited state. Various models have been proposed to explain the mechanism of formation and the final structure of the intramolecular charge-transfer state.

The first model proposed by Grabowski et al.,[19,20] commonly named TICT for twisted intramolecular charge transfer, supposes the existence of two conformers for the intramolecular charge-transfer excited state. After absorption, the promoted state starts in a nontwisted conformation. This conformation follows the twisting motion hypersurface and transforms into a twisted structure, which is a local minimum on the potential energy surface. This transformation is performed through a radiationless process. In the final conformation, the donor group is typically perpendicular to the phenyl ring presenting thus a complete electronic decoupling. This model is based on the observation that molecules with a twisted ground-state geometry, such as *N,N*-3,5-tetramethyl-4-aminobenzonitrile (TMAB-CN), only present the abnormal band, while systems such as 2,3,6,7-tetra-hydro-1*H*,5*H*-pyrido[3,2,1-*ij*]quinoline-9-carbonitrile (JULCN) or 1-ethyl-2,3-dihydro-1*H*-indole-5-carbonitrile (EIN) (see Figure 1), where the rotation of the N atom is restricted, only show the normal band. However, this model cannot predict the absence of dual fluorescence in systems such as 3-(*N,N*-dimethylamino)benzonitrile (3DMAB-CN),[2,14,18] where the rotation of the amino group is still possible. It also does not explain the dual fluorescence of NMC7.

The planar intramolecular charge-transfer (PICT) model[2,12,13,18,21] has been proposed as an alternative to explain the presence of dual fluorescence in seven-membered ring systems,[18] such as NMC7, in which the donor group cannot
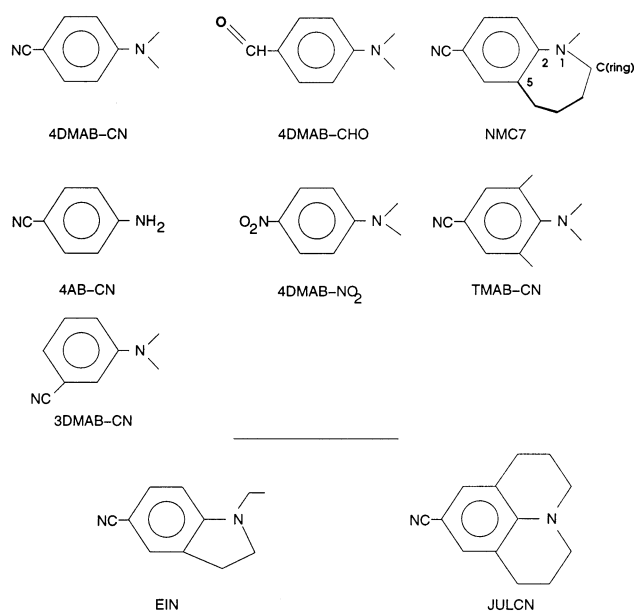

Figure 1. (a) Molecules investigated in this paper. 4DMAB-CN, 4DMAB-CHO, and NMC7 do exhibit the dual fluorescence phenomenon, while the others, 4AB-CN, 3DMAB-CN, 4DMAB-NO$_2$, and TMAB-CN, do not. (b) EIN and JULCN do not present dual fluorescence because the donor group is prevented from twisting.

fully rotate. Contrary to the twisting ICT model where only one initial state is involved in the formation of the "final" intramolecular charge-transfer state, the planar ICT model supposes the existence of a solvent-induced vibronic coupling through the N-inversion mode of the amino group between the two initial singlet states resulting in a more stabilized planar structure. The final intramolecular charge-transfer state is characterized by a quinoïdal structure with a configurational change of the amino nitrogen and with a shortened benzene−amino bond length, preventing thus the twisting between these two subunits. In this structure, the nitrogen lone pair becomes part of the π electron system of the phenyl ring, leading thus to a positive charge on the donor group and a negative charge on the acceptor moiety, hence the existence of an intramolecular charge-transfer state with a large dipole moment. The existence of an electronic coupling in the planar ICT model is in total contradiction with the twisting ICT model. This point has been recently discussed in refs 13 and 15.

In the planar ICT model, two requirements have to be fulfilled to observe the dual fluorescence. First, the energy gap between the two initial states has to be small enough to allow vibronic coupling, no matter which state is more stable. According to Zachariasse et al.,[18] this explains why dual fluorescence is observed for compounds such as 4DMAB-CN and 4DMAB-CHO but not for 4AB-CN, 4DMAB-NO$_2$, or 3DMAB-CN where this energetic gap is too large. Second, the energy barrier to the rehybridization of the amino nitrogen from pyramidal to planar has to be small enough to allow the formation of the intramolecular charge-transfer state. For example, three-membered ring compounds show only normal L_b emission (high energy barrier), while dual fluorescence occurs for seven-membered ring compounds (low energy barrier). However, no direct experimental proof of either model has been obtained up to now, and the mechanism of formation of the charge-transfer excited state is still under debate.

(8) Rotkiewicz, K.; Grabowski, Z. R.; Krowczynski, A.; Kiihnle, W. *J. Lumin.* **1976**, *12/13*, 877.
(9) Dobkowski, J.; Kirkor-Kaminska, E.; Koput, J.; Siemiarczuk, A. *J. Lumin.* **1982**, *27*, 339.
(10) Rettig, W.; Rotkiewicz, K.; Rubaszewska, W. *Spectrochim. Acta* **1984**, *40A*, 241.
(11) Schuddeboom, W.; Jonker, S. A.; Warman, J. M.; Leinhos, U.; Kiihnle, W.; Zachariasse, K. A. *J. Phys. Chem.* **1992**, *96*, 10809.
(12) Zachariasse, K. A.; Grobys, M.; Tauer, E. *Chem. Phys. Lett.* **1997**, *274*, 372.
(13) Il'ichev, Y. V.; Kühnle, W.; Zachariasse, K. A. *J. Phys. Chem. A* **1998**, *102*, 5670.
(14) Rettig, W.; Bliss, B.; Dirnberger, K. *Chem. Phys. Lett.* **1999**, *305*, 8.
(15) Zachariasse, K. A. *Chem. Phys. Lett.* **2000**, *320*, 9.
(16) Rettig, W.; Zietz, B. *Chem. Phys. Lett.* **2000**, *317*, 187.
(17) Bulliard, C.; Allan, M.; Wirtz, G.; Haselbach, E.; Zachariasse, K. A.; Detzer, N.; Grimme, S. *J. Phys. Chem. A* **1999**, *103*, 7766.
(18) Zachariasse, K. A.; Grobys, M.; von der Haar, Th.; Hebecker, A.; Il'ichev, Yu. V.; Morawski, O.; Rücker, I.; Kiihnle, W. *J. Photochem. Photobiol., A* **1997**, *105*, 373.
(19) Rotkiewicz, K.; Grellmann, K. H.; Grabowski, Z. R. *Chem. Phys. Lett.* **1973**, *19*, 315; *Chem. Phys. Lett.* **1973**, *21*, 212.
(20) Grabowski, Z. R.; Rotkiewicz, K.; Siemiarezuk, A.; Cowley, D. J.; Baumann, W. *Nouv. J. Chim.* **1979**, *3*, 443.
(21) von der Haar, Th.; Hebecker, A.; Il'ichev, Yu. V.; Jiang, Y.-B.; Kiihnle, W.; Zachariasse, K. A. *Recl. Trav. Chim. Pays-Bas* **1995**, *114*, 430.

Computational chemists have tackled this problem using various methodologies that either include[22–32] or ignore[1,17,33–40] solvent effects. 4DMAB-CN and, to a lesser extent, 4AB-CN have been favorite molecules due to their small size and the existence of experimental data.[2,11,17,20,41] Most theoretical calculations do support the twisting rather than planar intramolecular charge-transfer model. In addition to those two models, a third one, named the rehybridization intramolecular charge-transfer model, has been proposed by Domcke and co-workers[34,35,39] on the basis of their CIS and CASPT2 calculations. This model has been applied for linear acceptor groups such as $C\equiv N$ and $C\equiv CH$ where the change in carbon hybridization from sp $\rightarrow$ sp^2 is responsible for the energy stabilization.

Recently, time-resolved Raman spectra[42] of the charge-transfer state of 4DMAB-CN have been reported, also supporting the twisting ICT model. Another paper,[30] combining CASSCF calculations and time-resolved vibrational spectroscopy, concluded that a final statement between planar or twisting cannot be made even though their results are in favor of the twisting ICT model.

The time-dependent density functional theory (TDDFT) is now well-known as a rigorous formalism[43–46] for the treatment of excitation energies within the DFT framework. A few years ago, Casida et al.[47–49] have introduced a molecular formulation of TDDFT. The combination of efficiency, that is, computational cost, as well as precision, that is, a few tenths of an eV, even

for high-excited or Rydberg states when an asymptotically corrected v_{xc} is used,[50–53] makes TDDFT very attractive. It has been applied for the calculation of excitation energies of simple molecules[49–51,54–57] and large systems.[58–60] However, in cases where the ground-state description begins to break down, as is the case for dissociating molecules,[61–63] care has to be taken with practical TDDFT with approximate functionals. In addition, it has been noticed that excitations involving large changes in the charge density tend to be underestimated by TDDFT (even when the ground-state description appears to be adequate) because present day exchange-correlation functionals are in some sense too local. Furthermore, TDDFT has been shown to be a well-suited method to correctly treat avoided crossing, leading to the same quality results as the MRD-CI method.[64]

In this paper, we want to address the planar or twisting intramolecular charge-transfer issue for a set of dual (4DMAB-CN, 4DMAB-CHO, and NMC7) and nondual (4AB-CN, 3DMAB-CN, 4DMAB-NO$_2$, TMAB-CN) fluorescent molecules (see Figure 1) using the TDDFT method. TMAB-CN has been chosen because of the existence of experimental fluorescence spectra recorded in the gas phase, allowing thus a direct comparison between experimental and calculated emission energies. For both 4DMAB-CN and 4AB-CN, numerous theoretical calculations with various methods exist in the literature, and it is interesting to assess the quality of the TDDFT method in calculating the emission energy of the charge-transfer excited state. 3DMAB-CN, which is not dual fluorescent, will be compared to 4DMAB-CN because they both have the same donor and acceptor groups. NMC7 and TMAB-CN will be analyzed in parallel because both have a twisted ground-state geometry but a different fluorescence behavior. Finally, 4DMAB-CHO and 4DMAB-NO$_2$ are planar molecules being dual and nondual fluorescent, respectively. In this study, only singlet excited states will be investigated, and thus other patterns of deactivation via triplet states leading to phosphorescence emission are not treated herein.

In a previous paper, we have discussed the reliability of the TDDFT method in the calculation of absorption spectra involving charge-transfer excited states.[65] It has been concluded that for nontwisted ground-state molecules, agreement within 0.11 eV could be obtained when the B3LYP functional is used.

(22) Kato, S.; Amatasu, Y. *J. Chem. Phys.* **1990**, *92*, 7241.
(23) Broo, A.; Zerner, M. C. *Chem. Phys. Lett.* **1994**, *227*, 551.
(24) Gorse, A.-D.; Pesquer, M. *J. Phys. Chem.* **1995**, *99*, 4039.
(25) Scholes, G. D.; Phillips, D.; Gould, I. R. *Chem. Phys. Lett.* **1997**, *266*, 521.
(26) Gedeck, P.; Schneider, S. J. *J. Photochem. Photobiol., A* **1997**, *105*, 165.
(27) Scholes, G. D.; Gould, I. R.; Parker, A. W.; Philips, D. *Chem. Phys.* **1998**, *234*, 21.
(28) Purkayastha, P.; Bhattacharyya, P. K.; Bera, S. C.; Chattapadhyay, N. *Phys. Chem. Chem. Phys.* **1999**, *1*, 3253.
(29) Gedeck, P.; Schneider, S. J. *J. Photochem. Photobiol., A* **1999**, *121*, 7.
(30) Dreyer, J.; Kummrow, A. *J. Am. Chem. Soc.* **2000**, *122*, 2577.
(31) Mennucci, B.; Toniolo, A.; Tomasi, J. *J. Am. Chem. Soc.* **2000**, *122*, 10621.
(32) Sudholt, W.; Staib, A.; Sobolewski, A. L.; Domcke, W. *Phys. Chem. Chem. Phys.* **2000**, *2*, 4341.
(33) Gorse, A.-D.; Pesquer, M. *J. Mol. Struct.* **1993**, *281*, 21.
(34) Sobolewski, A. L.; Domcke, W. *Chem. Phys. Lett.* **1996**, *259*, 119.
(35) Sobolewski, A. L.; Domcke, W. *Chem. Phys. Lett.* **1996**, *250*, 428.
(36) Parusel, A. B. J.; Kohler, G.; Grimme, S. *J. Phys. Chem. A* **1998**, *102*, 6297.
(37) Parusel, A. B. J.; Kohler, G.; Nooijen, M. *J. Phys. Chem. A* **1999**, *103*, 4056.
(38) Parusel, A. B. J. *Phys. Chem. Chem. Phys.* **2000**, *24*, 5545.
(39) Sobolewski, A. L.; Sudholt, W.; Domcke, W. *J. Phys. Chem. A* **1998**, *102*, 2716.
(40) Sudholt, W.; Sobolewski, A.; Domcke, W. *Chem. Phys.* **1999**, *240*, 9.
(41) Bauman, W.; Bischof, H.; Frohling, J. C.; Brittinger, C.; Rettig, W.; Rotkiewicz, K. J. *J. Photochem. Photobiol., A* **1992**, *64*, 49.
(42) Kwok, W. M.; Ma, C.; Matousek, P.; Parker, A. W.; Phillips, D.; Toner, W. T.; Towrie, M. *Chem. Phys. Lett.* **2000**, *322*, 395.
(43) Gross, E. K. U.; Kohn, W. *Adv. Quantum Chem.* **1990**, *21*, 255.
(44) Gross, E. K. U.; Ullrich, C. A.; Gossmann, U. J. In *Density Functional Theory*; Gross, E. K. U., Dreizler, R. M., Eds.; NATA ASI Series; Plenum: New York, 1994; p 149.
(45) Gross, E. K. U.; Dobson, J. F.; Petersilka, M. In *Density Functional Theory*; Nalewajski, R. F., Ed.; Springer Series "Topics in Current Chemistry"; Springer: Heidelberg, 1996; Vol. 81, p 81.
(46) Burke, K.; Gross, E. K. U. In *Density Functionals: Theory and Applications. Proceedings of the Tenth Chris Engelbrecht Summer School in Theoretical Physics*; Joubert, D., Ed.; Springer Lecture Notes in Physics; Springer: Berlin, 1997.
(47) Casida, M. E.; Jamorski, C.; Bohr, F.; Guan, J.; Salahub, D. R. In *Theoretical and Computational Modeling of NLO and Electronic Materials*; Karna, A. P., Yeates, A. T., Eds.; American Chemical Society: Washington, DC, 1996 (Proceedings of ACS Symposium, Washington, DC, 1994); p 145.
(48) Casida, M. E. In *Recent Advances in Density Functional Methods, Part I*; Chong, D. P., Ed.; World Scientific: Singapore, 1995; p 155.
(49) Jamorski, C.; Casida, M. E.; Salahub, D. R. *J. Chem. Phys.* **1996**, *104*, 5134.

(50) Casida, M. E.; Jamorski, C.; Casida, K. C.; Salahub, D. R. *J. Chem. Phys.* **1998**, *11*, 4439.
(51) Tozer, D. J.; Handy, N. C. *J. Chem. Phys.* **1998**, *109*, 10180.
(52) Handy, N. C.; Tozer, D. J. *J. Comput. Chem.* **1999**, *20*, 106.
(53) Tozer, D. J.; Amos, R. D.; Handy, N. C.; Roos, B. J.; Serrano-Andres, L. *Mol. Phys.* **1999**, *97*, 859.
(54) Petersilka, M.; Gossmann, U. J.; Gross, E. U. K. *Phys. Rev. Lett.* **1996**, *76*, 1212.
(55) Bauernschmitt, R.; Haeser, M.; Treutler, O.; Ahlrichs, R. *Chem. Phys. Lett.* **1997**, *264*, 573.
(56) van Gisbergen, S. J. A.; Kootstra, F.; Schipper, P. R. T.; Gritsenko, O. V.; Snijders, J. G.; Baerends, E. J. *Phys. Rev. A* **1998**, *57*, 2556.
(57) Stratmann, R. E.; Scuseria, G. E.; Frisch, M. J. *J. Chem. Phys.* **1998**, *109*, 8218.
(58) Sundholm, D. *Chem. Phys. Lett.* **1999**, *302*, 480.
(59) Bauernschmitt, R.; Ahlrichs, R.; Hennrich, F. H.; Kappes, M. M. *J. Am. Chem. Soc.* **1998**, *120*, 5052.
(60) van Gisbergen, S. J. A.; Schipper, P. R. T.; Gritsenko, O. V.; Baerends, E. J.; Snijders, J. G.; Champagne, B.; Kistman, B. *Phys. Rev. Lett.* **1999**, *83*, 694.
(61) Cai, Z.-L.; Reimers, J. R. *J. Chem. Phys.* **2000**, *112*, 527.
(62) Casida, M. E.; Gutierrez, F.; Guan, J.; Gadea, F.-X.; Salahub, D. R.; Daudey, J.-P. *J. Chem. Phys.* **2000**, *113*, 7062.
(63) Gritsenko, O. V.; van Gisbergen, S. J. A.; G6rling, A.; Baerends, E. J. *J. Chem. Phys.* **2000**, *113*, 8478.
(64) Casida, M. E.; Casida, K. C.; Salahub, D. R. *Int. J. Quantum Chem.* **2002**, *70*, 933.
(65) Jamorski, C.; Foresman, J. B.; Thilgen, C.; Liithi, H.-P. *J. Chem. Phys.* **2002**, *116*, 8716.
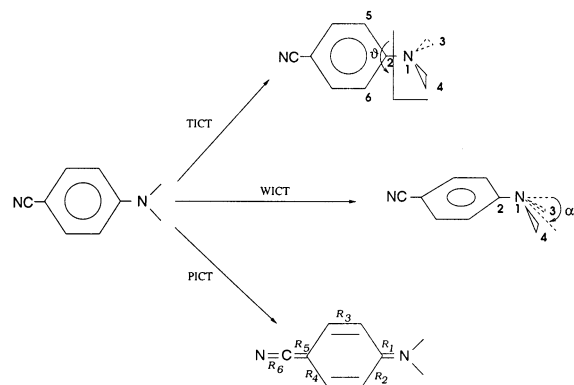
Figure 2. Schematic representation of the various mechanisms investigated in this paper. The TICT model is represented by the variation of the twist angle, $\theta = \theta_1 + \theta_2/2$, where $\theta_1 = \angle_{3-1-2-5}$ and $\theta = \angle_{4-1-2-6}$. The WICT mechanism proposes a relaxation mode according to the wagging angle $\alpha = 180 - \angle_{3-1-2-4}$. The PICT mechanism corresponds to a structural change of the molecule toward a quinoïdal structure.

However for nonplanar molecules, like TMAB-CN, better results are obtained when the MPW1PW91 functional is used (0.17 eV agreement with gas-phase experimental data for the charge-transfer excitation energy).

All three possible mechanisms (see Figure 2) will be investigated for all molecules using various functionals (B3LYP and MPW1PW91), providing thus a large set of comparisons. From these data, it will be possible to distinguish which mechanism leads to a stable charge-transfer excited state responsible for the L_a band present in the fluorescence spectra.

II. Computational Details

All calculations have been performed using the Gaussian 98 package.[66] A 6-31G(d)[67] and a 6-311+G(2d,p)[68,69] basis set have been used in our calculations. The exponent used for the polarization function of the first-row atoms with the 6-31G(d) basis set is $\alpha^d = 0.8$, while for the 6-311+G(2d,p) basis set the following values are used: $\alpha^d_N = 0.1826, 0.4565, \alpha^d_C = 0.1252, 0.313, \alpha^d_O = 0.646, 0.2584,$ and $\alpha^d_P = 0.75$. These two basis sets will be referred to later on as Sm and Bg, respectively. Geometries have been optimized for the ground state with the B3LYP[70] and MPW1PW91[71] functionals. Geometries were computed by requiring all forces to be less than 0.005 au, and the displacements predicted by the next step were required to be less than 0.002 au. Energies and densities have been obtained through the resolution of the Kohn−Sham equation using the B3LYP or MPW1PW91 functional. Convergence criteria for the energy and for the density are 10^{-7} and 10^{-5} au, respectively. The grid used to calculate the exchange and correlation potential is pruned and composed of 75 radial shells and 302 angular points. Excitation energies were calculated using the TDDFT implementation in Gaussian.[57] Here, dipole moments for

excited states were computed using the one-particle density matrix. These are formed by transforming the $(X + Y)$ CI vectors into the atomic orbital basis (see Stratmann et al.[57] for the definition of X and Y). This is an approximation, which typically results in a slight overestimation of the dipole moment (our results will confirm this). The true dipole moment could be calculated, using the Hellmann−Feynman theorem, as an expectation value over the charge density. Such calculations were not performed herein. Still, our approximate dipole moments will be useful when comparing one state to another.

Calculations where geometries and excitation energies have been obtained using the same basis set and functional are the most consistent from a methodological point of view. In the tables of this paper, excitation energy calculations are identified by the geometry optimization level, the functional used, and the basis set that has been chosen. The following general notation has been adopted: Opt − b1/Func − b2, where Opt represents the functional used in the geometry optimization, Func for the functional used to calculate excited-state energies, and b1, b2 specify the basis set in each case. This notation reduces to a shorter form when b1 = b2 or Opt = Func or Opt − b1 = Func − b2. For example, B3LYP-Sm/B3LYP-Bg will be written B3LYP-(Sm/Bg), and B3LYP-Sm/B3LYP-Sm will simply be written B3LYP-Sm. Also, the MPW1PW91-(Sm/Bg) notation has been written in the abbreviated form MPW91-(Sm/Bg) in all tables of this paper.

For all molecules, excitation energies are calculated low enough, as compared to first ionization energy, to be considered as reasonable. For example, at the B3LYP-(Sm/Bg) level, $-\epsilon_{HOMO}$ is equal to 5.92 eV (4DMAB-CN), 6.39 eV (4AB-CN), 5.93 eV (3DMAB-CN), 5.84 eV (4DMAB-CHO), 6.16 eV (4DMAB-NO$_2$), 6.13 eV (TMAB-CN), and 6.34 eV (NMC7).

Computed excitation energies correspond to vertical excitation energies without the zero-point energy correction.

The various mechanisms that will be investigated are displayed in Figure 2. The wagging motion, α, is described by the variation of the following dihedral angle $\alpha = (180 - \angle_{3-1-2-4})°$. The potential energy surface has been investigated according to the variation of α from 0° to 30° with a step of 10°. For 4AB-CN, the surface has been investigated up to $\alpha = 60°$ because, at the B3LYP computed equilibrium geometry, α^0 is equal to 30.104°. This motion corresponds to the change in hybridization of the amino nitrogen from pyramidal to planar. Structural change of the molecule toward a planar quinoïdal molecule has also been investigated (planar ICT model). In this case, some bonds are stretched (R_2, R_4, R_6), while others are shortened (R_1, R_3, R_5) according to the following relation: $R_j^i = R_j^0 (1 \pm x^i)$, where $0 \le x^i < 0.1$, step is 0.02, and R_j^0 corresponds to jth optimized bond length. Finally, the twisted motion is described by the rotational angle θ, which varies from 0 to 180° with a step of 10° for most of the molecules of this study. θ is defined by $(\theta_1 + \theta_2)/2$, where θ_1 represents the dihedral angle $\angle_{3-1-2-5}$, and θ_2 corresponds to $\angle_{4-1-2-6}$ (see Figure 2). The potential energy surface will be explored according to the variation of θ from its optimized ground-state value, θ^0.

This study is limited in the sense that it only corresponds to a scan of the potential energy surface along the above-mentioned parameters and that no excited-state geometry optimization has been performed.

III. Results

A. The Potential Curves of 4DMAB-CN, 4AB-CN, and 3DMAB-CN. The emission spectra of 4DMAB-CN and 4AB-CN have been recorded by several authors showing that the former is dual fluorescent in nonpolar solvents, whereas the latter is not, even in polar solvents. Because of their different behavior and their small size, these two molecules have been thoroughly investigated by computational chemists. A great number of calculations of their emission spectra using CASPT2,[1,32,34,35,39] DFT/SCI,[36] STEOM,[37] and DFT/MRCI[38] do exist in the literature.

(66) Frisch, M. J.; Trucks, G. W.; Schlegel, H. B.; Scuseria, G. E.; Robb, M. A.; Cheeseman, J. R.; Zakrzewski, V. G.; Montgomery, J. A., Jr.; Stratmann, R. E.; Burant, J. C.; Dapprich, S.; Millam, J. M.; Daniels, A. D.; Kudin, K. N.; Strain, M. C.; Farkas, O.; Tomasi, J.; Barone, V.; Cossi, M.; Cammi, R.; Mennucci, B.; Pomelli, C.; Adamo, C.; Clifford, S.; Ochterski, J.; Petersson, G. A.; Ayala, P. Y.; Cui, Q.; Morokuma, K.; Malick, D. K.; Rabuck, A. D.; Raghavachari, K.; Foresman, J. B.; Cioslowski, J.; Ortiz, J. V.; Stefanov, B. B.; Liu, G.; Liashenko, A.; Piskorz, P.; Komaromi, I.; Gomperts, R.; Martin, R. L.; Fox, D. J.; Keith, T.; Al-Laham, M. A.; Peng, C. Y.; Nanayakkara, A.; Gonzalez, C.; Challacombe, M.; Gill, P. M. W.; Johnson, B. G.; Chen, W.; Wong, M. W.; Andres, J. L.; Head-Gordon, M.; Replogle, E. S.; Pople, J. A. *Gaussian 98*; Gaussian, Inc.: Pittsburgh, PA, 1998.
(67) Hehre, W. J.; Ditchfield, R.; Pople, J. A. *J. Chem. Phys.* **1972**, *56*, 2257.
(68) Krishnan, R.; Binkley, J. S.; Seeger, R.; Pople, J. A. *J. Chem. Phys.* **1980**, *72*, 650.
(69) Frisch, M. J.; Pople, J. A.; Binkley, J. S. *J. Chem. Phys.* **1984**, *80*, 3265.
(70) Becke, A. D. *J. Chem. Phys.* **1993**, *98*, 5648.
(71) Adamo, C.; Barone, V. *J. Chem. Phys.* **1998**, *108*, 664.

Table 1. Experimental and Computed Singlet Excitation Energies (eV), Oscillator Strengths, *f*, and Dipole Moments, μ (D), for 4DMAB-CN Using Various Functionals (Emission Energies Have Been Calculated at the Perpendicular Optimized Ground-State Geometry (TICT); the Reader Is Referred to Ref 65 for the B3LYP Absorption Energies)

| | | emission | | | | | |
| | G.S.[a] | 1A → CT | | | 1B → LE | | |
methods	μ	ΔE	f	μ	ΔE	f	μ
exp[b]	5−7	3.33[c]		14−20	3.64		
CASPT2[1]	5.10	3.74	0.00	15.45	4.58	0.01	4.87
CASPT2[1]	5.75	3.94	0.00	15.61	4.55	0.00	5.70
CASPT2[32]		3.72			3.82		
STEOM[37]	5.2	4.0	0.00	16.3	4.6	0.00	5.4
DFT/SCI[36]	5.5	3.4	0.00	19.3	4.5	0.00	5.9
DFT/MRCI[38]		4.06			4.77		
B3LYP-(Sm/Bg)[d,e]	5.67	3.09	0.00	20.16	3.95	0.00	18.53
B3LYP-(Sm/Bg)[d,f]	5.63	3.19	0.00	20.15	4.03	0.00	18.50
MPW91-(Sm/Bg)[d,g]	5.70	3.27	0.00	19.62	4.15	0.00	18.25

[a] G.S. stands for ground state. [b] See the following references: 2, 11, 12, 20, 41, 72−74. [c] This value has been measured in *n*-hexane. In the gas phase, this value is expected to be higher (between 3.53 and 3.63 eV). [d] See Computational Section for more details about the notation used here. [e] Results for the nonwagged molecule ($\alpha = 0°$). For the ground state, an energy increase of 0.59 eV is calculated at $\theta = 90°$ as compared to the optimized ground state at $\theta = 0°$. [f] Results for the wagged molecule ($\alpha = 20°$). For the ground state, an energy increase of 0.52 eV is calculated at $\theta = 90°$ as compared to the optimized ground state at $\theta = 0°$. [g] Results for the nonwagged molecule ($\alpha = 0°$). For the ground state, an energy increase of 0.59 eV is calculated at $\theta = 90°$ as compared to the optimized ground state at $\theta = 0°$. The MPW91-(Sm/Bg) 1B(LE) and 1A(CT) absorption energies have been calculated at 4.47 and 4.71 eV, respectively.

Experimental emission spectra and calculated excitation energies[2,11,12,20,41,72−74] for 4DMAB-CN at the twisted ground-state structure as well as their corresponding computed dipole moments and oscillator strengths are reported in Table 1.

Molecular orbitals of the electronic ground state structure and of the corresponding twisted geometry ($\theta = 90°$) are displayed in Figure 3. In its electronic ground state, 4DMAB-CN has an optimized geometry with a C_{2v} symmetry. In the absorption spectrum, the first excited state, which describes the promotion from the donor group (π_{donor}) to the benzene moiety (π^*_{phenyl}), will be noted 1B. The second excited state, which corresponds to the transition from the donor (π_{donor}) to the acceptor group ($\pi_{acceptor}$), will be called 1A (see ref 65).

The potential energy surface of the ground and low-lying singlet excited states of 4DMAB-CN along the twisting coordinate, θ, is presented in Figure 4. The ground-state energy increases along the twisting path reaching a maximum at $\theta = 90°$, and a crossing appears between the first and second excited states. The energy of the 1B state has its minimum value at $\theta = 0°$ (the ground-state optimized geometry) and reaches a maximum value at $\theta = 90°$. The energy profile of the 1A state presents a minimum at the perpendicular structure, and it represents the lowest excited state along the twisting angle.

The nature of the 1A state changes along the twisting path, reaching a full charge-transfer character for the perpendicular structure as it is reflected by the change in the oscillator strength values (see Table 1).

(72) Rettig, W.; Braun, D.; Suppan, P.; Vauthey, E.; Rotkiewicz, K.; Luboradzki, R.; Suwifiska, K. *J. Phys. Chem.* **1993**, *97*, 13500.
(73) Chattopadhyay, N.; Rommends, J.; Van der Auweraer, M.; de Schryver, F. C. *Chem. Phys. Lett.* **1997**, *264*, 265.
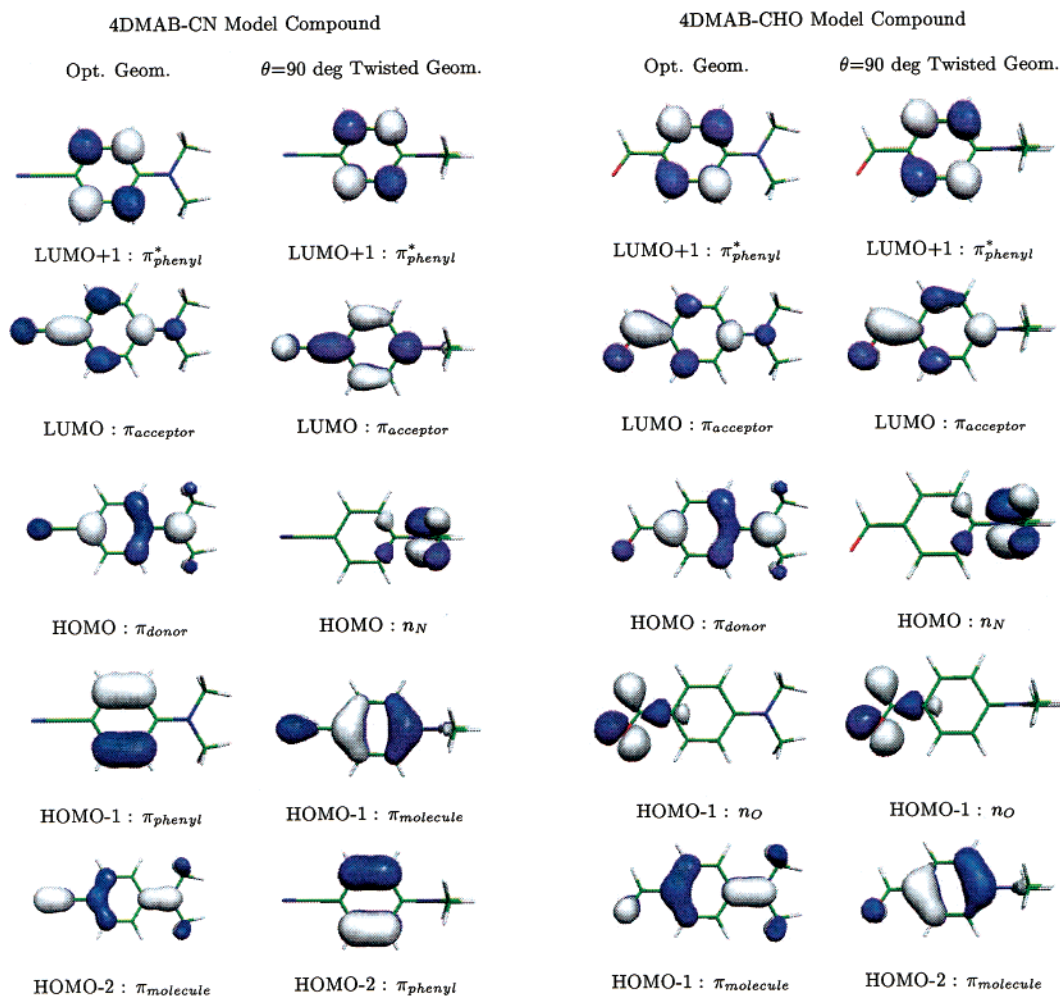(74) Guinther, R.; Oelkrug, D.; Rettig, W. *J. Chem. Phys.* **1993**, *97*, 8512.

Our TDDFT results along the twisting angle are in agreement with other theoretical calculations performed using CASPT2 (with a wagged molecule, $\alpha = 21°$) and DFT/MRCI methods. On the other hand, DFT/SCI and CASPT2 results (with a nonwagged molecule, $\alpha = 0°$) predict an energy minimum at $\theta = 60°$ for the first excited state. In Figure 4, calculations performed with a wagging angle ($\alpha = 20°$) are also displayed for several twisting angles $\theta = \{0°, 30°, 60°, 90°\}$. In this case, the C_2 axis is not an element of symmetry of the molecule anymore, and therefore an avoided crossing occurs between the first and second excited states because they have the same irreducible representation. For the wagged molecule, the energy barrier present on the potential energy surface of the first excited state that separates the two minima ($\theta = 0$ and $90°$) resulting from the avoided crossing is calculated at 0.04 eV using the B3LYP-(Sm/Bg) method. CASPT2 and DFT/MRCI calculations report a value of 0.13 and 0.27 eV, respectively. It has to be restated that this energy barrier is only an estimation of the true energy barrier because it only represents a nonrelaxed scan along the twisting angle. Estimation of the true energy barrier would require the knowledge of the energy of the optimized twisted charge-transfer excited state, as well as the energy of the transition state along the path from the ground- to the charge-transfer excited state optimized structure. Therefore, only methodological comparisons are meaningful in this case.

Within the twisting ICT model, the L_a fluorescence emission is supposed to take place from the twisted 1A excited state. Our calculated values are 3.09 and 3.27 eV with B3LYP-(Sm/Bg) and MPW91-(Sm/Bg) methods, respectively (see Table 1). Experimental measurements in cyclohexane observe this L_a band at 3.33 eV. The estimation of this band in the gas phase shall raise its energy by 0.2 eV to 0.3 eV, yielding thus an emission energy between 3.53 and 3.63 eV. CASPT2 results vary from 3.72 (using a large active space)[32] to 3.94 eV from the earlier calculation of Serrano et al.[1] Among all theoretical results presented in Table 1, CASPT2 results yield the best agreement with the experimental L_a emission energy. The B3LYP calculated dipole moment of the ground and 1A excited states decreases, respectively increases, monotonically along the twisting path, in agreement with other theoretical calculations.

Contrary to 4DMAB-CN, 4AB-CN is a nonplanar system, and therefore symmetry could not be used to identify the various excited states. The potential energy surfaces of the ground and low-lying singlet states of 4AB-CN along the twisting path are displayed in Figure 5. There is an avoided crossing at $\theta = 50°$ between the first (1S) and second (2S) excited states. Therefore, the nature of both 1S and 2S excited states, that are described in absorption by the following electronic transition $\pi_{donor} \rightarrow \pi^*_{phenyl}$ and $\pi_{donor} \rightarrow \pi_{acceptor}$, respectively, will change after the avoided crossing. At $\theta = 90°$, the 1S state is described by the electronic promotion from $n_N \rightarrow \pi_{acceptor}$, and the 2S state is associated to the electronic transition from $n_N \rightarrow \pi^*_{phenyl}$. The energy profile of the first excited state, 1S, presents two minima at $\theta = 0°$ and at $\theta = 90°$, whereas the 2S one shows a minimum at $\theta = 0°$ and a maximum at $\theta = 90°$. In the case of 4AB-CN, the first excited-state energy profile presents the lowest minimum at the optimized ground-state structure, whereas for 4DMAB-CN, the lowest minimum is associated with the twisted

Figure 3. Molecular orbitals for the optimized ground-state structure and for the twisted conformer of 4DMAB-CN (left) and 4DMAB-CHO (right). The molecular orbitals computed for 4AB-CN, 3DMAB-CN, TMAB-CN, and NMC7 are similar to those of 4DMAB-CN. The molecular orbitals of 4DMAB-NO$_2$ are similar to those of 4DMAB-CN except the HOMO−2 which is described by a combination of the lone-pair orbitals of the oxygen.

conformation of the 1A state. All other theoretical calculations are in agreement with this picture.

Table 2 reports the experimental dipole moment and calculated emission energies for the twisted conformation as well as the corresponding computed dipole moments and oscillator strengths. In our previous paper,[65] it was shown that B3LYP computed absorption energies (4.57 and 5.06 eV) compared well with "hypothetical" gas-phase values estimated at 4.45 and 4.86 eV for the 1S and 2S excited states, respectively. In agreement with other theoretical results, the twisted 1S excited state ($\theta =$ 90°) is calculated higher than the optimized conformation ($\theta^0 = 0°$), with both B3LYP-(Sm/Bg) and MPW91-(Sm/Bg) methods. Our calculated emission energies from the twisted 1S state are between CASPT2 (with a wagged molecule) and DFT/SCI results. The B3LYP calculated dipole moments of the ground and second excited states decrease along the twisting angle, whereas the one of the first excited state increases along the same coordinate. The other theoretical results observed the same variation.

The potential energy surface of the ground and low-lying states of 4DMAB-CN and 4AB-CN according to the wagging motion has also been explored using the TDDFT method, see Figure 6. In agreement with both CASPT2 and DFT/SCI results, the "planar" charge-transfer state of both 4DMAB-CN and 4AB-CN molecules does not stabilize along this motion path. This shows that this mechanism is unable to explain the L$_a$ band present in the fluorescence spectra as well as its strong dependence on solvent polarity.

To complete the study, the potential energy surfaces of 4DMAB-CN and 4AB-CN have also been calculated along the structural change of the molecule toward a final quinoïdal structure, see Figure 7 (see Computational Section for more details about the chosen coordinates). Within the planar ICT model, the fluorescence is supposed to take place from a final quinoïdal structure that results from the coupling of both locally and charge-transfer excited states according to the change in the configuration of the amino group toward planarity. In the case of the 4DMAB-CN molecule, the ground-state energy increases along this coordinate, and the first and second excited-state surfaces present a crossing at $x =$ 0.02. For higher values of x, excited-state energies increase, and no stabilization in energy for the charge-transfer excited state is observed along this structural change coordinate. In the case of the 4AB-CN molecule, the computed potential energy surface is similar to that computed for the 4DMAB-CN system. Therefore, this structural change could not be the mechanism that explains why the 4DMAB-CN molecule is dual fluorescent, whereas 4AB-CN is not, because
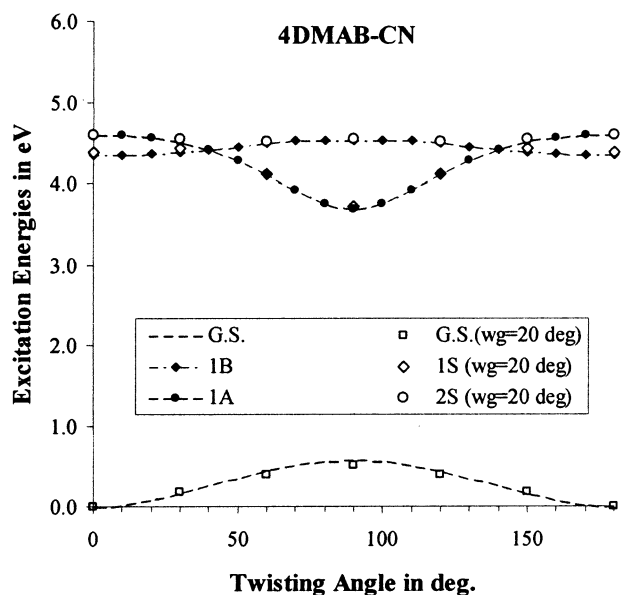
Figure 4. PES of the ground and low-lying singlet excited states of 4DMAB-CN along the twisting coordinate calculated with the B3LYP-(Sm/Bg) method. Results for a nonwagged molecule (symmetry C_2) and for a molecule with 20° wagging angle are shown.
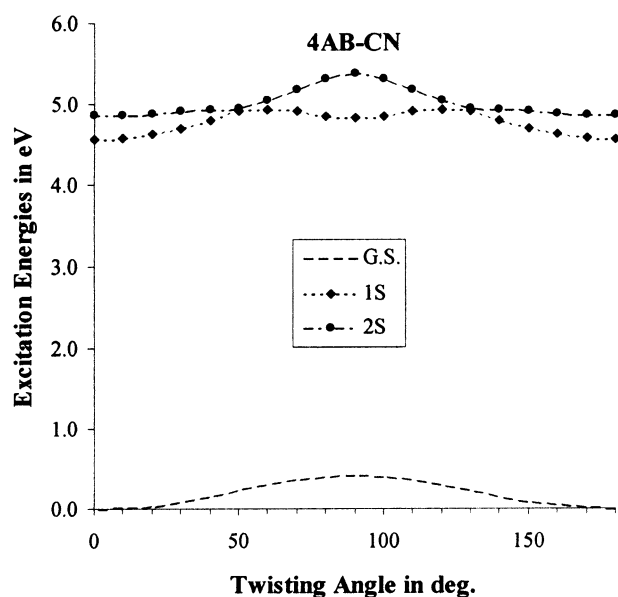

Figure 5. PES of the ground and low-lying singlet excited states of 4AB-CN along the twisting coordinate calculated with the B3LYP-(Sm/Bg) method.

both potential energy surfaces along this motion present similar behavior.

3DMAB-CN is an excellent test to compare to 4DMAB-CN because both have the same donor and acceptor groups while both show a different fluorescence behavior. Contrary to 4DMAB-CN, the ground-state optimized geometry of 3DMAB-CN computed at the B3LYP-(Sm/Bg) level is nonplanar ($\alpha^0 = 15.382°$ and $\theta^0 = 0°$). Experimentally, the absorption energy of 3DMAB-CN has been measured at 3.83 eV in *n*-hexane.[14] Table 3 displays experimental and calculated absorption and emission energies as well as their corresponding computed dipole moments and oscillator strengths. According to our calculations, the first vertical excited state corresponds to the charge-transfer state and is followed by the locally excited

Table 2. Experimental Dipole Moment and Computed Singlet Excitation Energies (eV) for the Twisted Conformation of 4AB-CN as Well as Their Calculated Oscillator Strengths, *f*, and Dipole Moments, μ (D), for 4AB-CN Using Various Functionals (Emission Energies Have Been Calculated at the Optimized Ground-State Geometry (TICT Model); the Reader Is Referred to Ref 65 for the B3LYP Absorption Energies)

| | | emission | | | | | |
| | G.S.[a] | 1S | | | 2S | | |
methods	μ	ΔE	f	μ	ΔE	f	μ
exp[2,11,20,41]	5−7						
CASPT2[1,b]	5.51	4.24	0.00	5.21	3.82	0.00	15.75
CASPT2[1,c]	4.86	4.10	0.01	4.65	4.54	0.00	15.65
STEOM[37]	5.1	4.6	0.00	5.3	5.1	0.00	14.5
DFT/SCI[36]	5.3	4.7	0.00	5.4	4.5	0.00	18.1
B3LYP-(Sm/Bg)[d,e]	5.33	4.41	0.00	18.79	4.97	0.00	5.57
MPW91-(Sm/Bg)[d,f]	5.39	4.57	0.00	18.26	5.10	0.01	5.67

[a] G.S. stands for ground state. [b] CASPT2 results with a wagging angle equal to 0°. For $\theta = 0°$, the 1S and 2S states correspond to the lB and 1A states, respectively, when the C2 symmetry is used. Within this symmetry, a crossing appears on the PES, and the 1S and 2S at $\theta = 90°$ correlate with the 1A and 1B states, respectively. [c] CASPT2 results with a wagging angle equal to 21°. [d] See Computational Section for more details about the notation used here. [e] For the ground state, an energy increase of 0.42 is calculated at $\theta = 90°$ as compared to the optimized ground state at $\theta = 0°$. [f] For the ground state, an energy increase of 0.44 is calculated at $\theta = 90°$ as compared to the optimized ground state at $\theta = 0°$. The MPW91-(Sm/Bg) 1S and 2S absorption energies have been calculated at 4.69 and 4.98 eV, respectively.

state. Absorption energies calculated with the MPW1PW91 functional show better agreement with the experimental value considering that the "hypothetical" gas-phase value is expected to be higher (3.98−4.08 eV) than the corresponding value in *n*-hexane.

Fluorescence spectra of 3DMAB-CN show only one band, even in polar solvents.[14] This band has been observed at 3.42 eV in *n*-hexane. This nondual fluorescence has been explained by Rettig et al.[14] by the prescence of a large energy gap between the 1S (having a locally excited character) and the 2S (having a charge-transfer character) excited states. According to these authors,[14] the charge-transfer excited state should be much higher in energy than the locally excited state such that even strong polar solvents could not lead to an energy stabilization large enough to bring the charge-transfer state below the locally excited state.

The potential energy surface of the ground and low-lying states of 3DMAB-CN according to the twisting mechanism is displayed in Figure 8. Contrary to the case of 4DMAB-CN, there is no crossing between the first and second excited states. On the other hand, the second and third excited states show an avoided crossing at $\theta = 35°$. Along the twisting coordinate, the charge-transfer excited state energy remains nearly constant. The energy of this state for the perpendicular conformation is calculated higher than the one of the optimized geometry conformation by 0.04 eV when the MPW91-(Sm/Bg) is used, whereas a 0.06 eV stabilization is computed with the B3LYP-(Sm/Bg) method. The dipole moment of the ground state decreases as the twisting angle increases. For the first excited state, the dipole moment increases along this coordinate, reaching a maximum of 18.53 D for $\theta = 90°$. This means that in a polar solvent, the twisted charge-transfer excited state should be more stabilized than the planar configuration. Therefore, emission might occur from the perpendicular charge-transfer excited state. In the case of the 3DMAB-CN molecule, we think
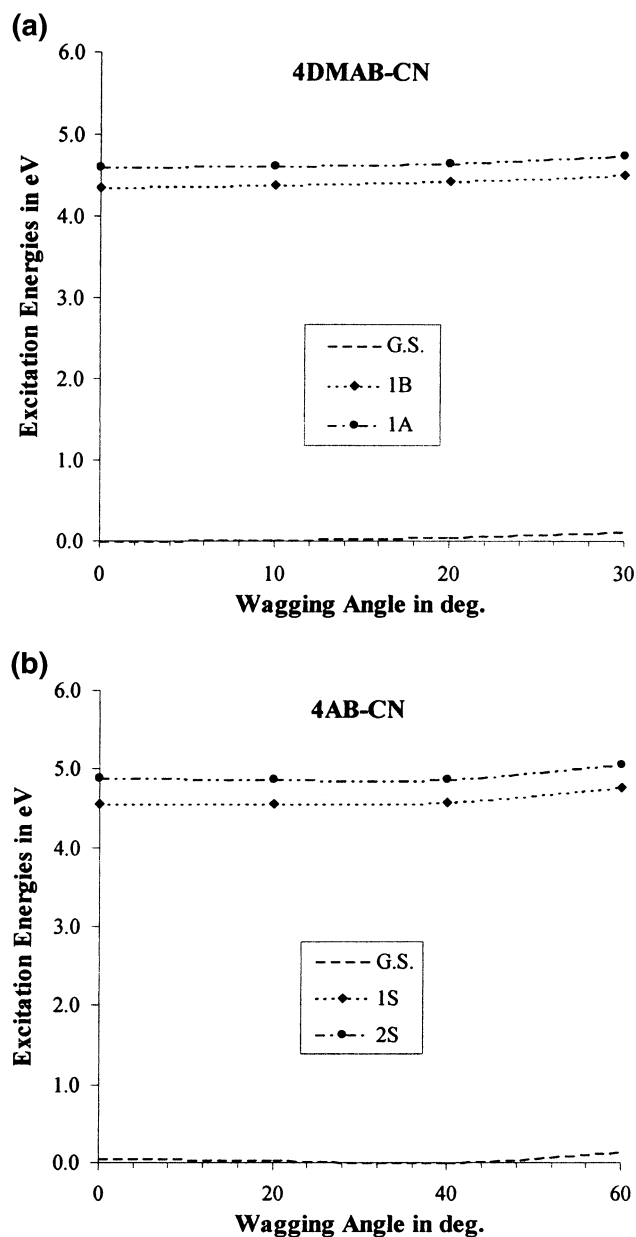
(a)

(a)

(b)

(b)

Figure 6. Computed PES using the B3LYP-(Sm/Bg) method as a function of the WICT coordinate for 4DMABN (a) and 4AB-CN (b).

Figure 7. Computed PES using the B3LYP-(Sm/Bg) method as a function of the PICT coordinate for 4DMABN (a) and 4AB-CN (b).

that more investigations are needed with various functionals and other ab initio methods to clearly establish the variation of the energy along the twisting coordinate.

For this molecule, the wagging motion has also been investigated, but is not reported in this paper because it leads to the same results as in the case of 4DMAB-CN. No stabilization in energy is computed for the charge-transfer excited state along the wagging coordinate. The planar motion has not been studied for this system, because it does not make sense to study the transition toward a quinoïdal structure of a compound with the acceptor group in the ortho position.

B. The Potential Curves of TMAB-CN and NMC7. Contrary to previous molecules of this study, TMAB-CN is a twisted ground state structure with a twisting angle, $\theta° = 114°$. The computed absorption spectrum has already been discussed in our previous paper[65] and compared to the most recent experimental gas-phase measurements[17] performed using the
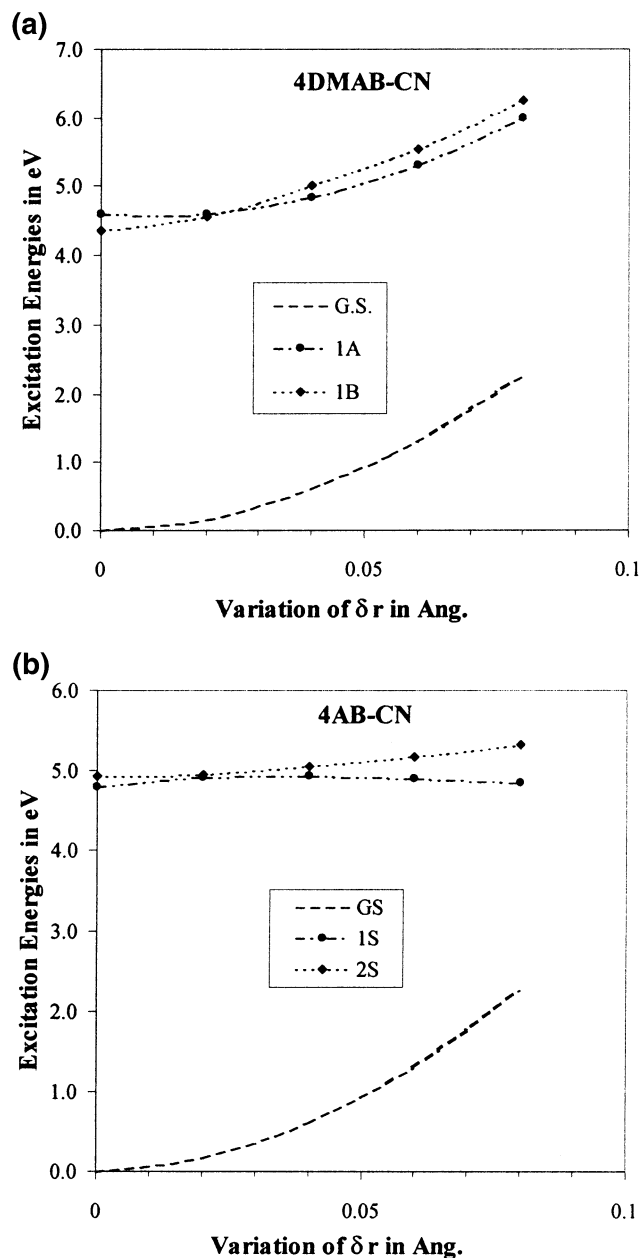
electron energy loss technique. It has been shown that for this molecule, results of better quality are obtained with the MPW1PW91 functional (4.10 eV) rather than with the B3LYP one (3.91 eV) when compared to experimental data (4.27 eV). DFT/SCI[17] computed excitation energies are in agreement with our TDDFT results. TMAB-CN is an interesting case because its fluorescence spectra is known in the gas phase. In emission, only one band has been observed, measured at 3.22 eV. Figure 9a displays the potential energy surface of the ground and low-lying states of TMAB-CN along the twisting coordinate. Contrary to 4DMAB-CN, the lowest singlet excited state, 1S, at the ground-state geometry has a charge-transfer character and corresponds to the transition from the donor (π_{donor}) to the acceptor ($\pi_{acceptor}$) group. The second excited state, 2S, is associated to the electronic promotion from the donor group (π_{donor}) to the benzene moiety (π^*_{phenyl}). The energy gap between these two excited states is calculated at 0.31 eV and at

Table 3. Experimental and Computed Singlet Excitation Energies (eV), Oscillator Strengths, f, and Dipole Moments, μ (D), for 3DMAB-CN Using Various Functionals (Absorption Energies Have Been Calculated at the Optimized Ground-State Geometry, and Emission Energies Have Been Computed at the Perpendicular Optimized Ground-State Geometry (TICT Model))

| | absorption | | | | | | | emission | | | | | | |
| | G.S.[a] | 1S → CT | | | 2S → LE | | | G.S.[a] | 1S → CT | | | 2S → LE | | |
methods	μ	ΔE	f	μ	ΔE	f	μ	μ	ΔE	f	μ	ΔE	f	μ
exp[14]		3.83[b]							3.42[c]					
B3LYP-(Sm/Bg)[d,e]	6.46	3.85	0.05	14.36	4.77	0.03	3.02	5.35	3.32	0.00	18.53	3.75	0.00	15.75
MPW91-(Sm/Bg)[d,f]	6.46	3.97	0.06	13.97	4.94	0.04	2.84	5.33	3.50	0.00	18.11	3.91	0.00	15.75

[a] G.S. stands for ground state. [b] Absorption measured in *n*-hexane; this value is expected to be higher in the gas phase (between 3.98 and 4.08 eV). [c] Emission measured in *n*-hexane. [d] See Computational Section for more details about the notation used here. [e] For the ground state, an energy increase of 0.47 eV is calculated at $\theta = 90°$ as compared to the optimized ground state at $\theta = 0°$. [f] For the ground state, an energy increase of 0.51 eV is calculated at $\theta = 90°$ as compared to the optimized ground state at $\theta = 0°$.
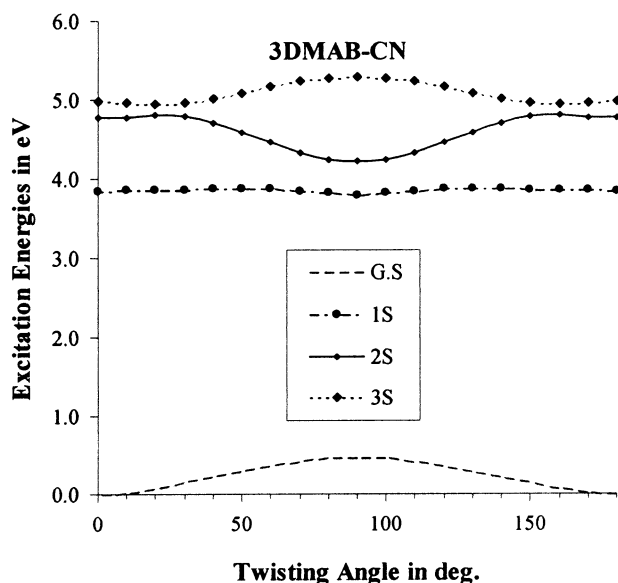

Figure 8. Ground and low-lying singlet states of the 3DMAB-CN molecule along the twisting path computed with the B3LYP-(Sm/Bg) method.

0.57 eV using the B3LYP-(Sm/Bg) and the MPW91-(Sm/Bg) methods, respectively, see ref 65. The 1S potential energy surface shows a minimum for the twisted structure at $\theta = 90°$, whereas the 2S energy profile locates a minimum at the optimized ground-state geometry ($\theta = 114°$).

The fluorescence emission from the twisted charge-transfer excited state is calculated at 3.56 and 3.72 eV using the B3LYP and MPW1PW91 functionals, respectively, which is too high compared to the gas-phase experimental value measured at 3.22 eV. One possible factor to explain this disagreement between calculated and measured emission spectra could be attributed to the fact that the geometry has not been reoptimized for each value of θ. However, we think that the general qualitative behavior of the potential energy surface along the twisting angle is well depicted within this approximation and that the stabilization of the charge-transfer state under this motion is in perfect agreement with the experimental fact, where only one band is measured in the fluorescence spectra. The dipole moment for the ground state decreases along the twisting angle, whereas it increases along the same coordinate for the first and second excited states.

The wagging motion has also been investigated for this molecule, and, as in previous cases, no minimum has been found for the 1S state, thus discrediting this mechanism as a possible explanation for the observed fluorescence.

The planar ICT model has not been investigated for TMAB-CN because the ground-state structure is already twisted. However, it can be seen on the energy profile of the charge-transfer excited state that the planar structure ($\theta = 0°$) is clearly higher in energy than the pretwisted optimized one ($\theta = 114°$). Therefore, motion toward a quinoïdal structure that would be more stable in energy than the twisted structure is very unlikely.

Like TMAB-CN, the 1-methyl-7-cyano-2,3,4,5-tetrahydro-1*H*-1-benzazepine (NMC7), see Figure 1, is already twisted in its ground-state geometry. At the computed equilibium geometry, the dihedral angle C5−C2−N1−C(ring), θ', is equal to 60.048° when the MPW91-(Sm/Bg) method is used. Tables 4 and 5 display experimental and calculated absorption and emisson energies as well as the computed oscillator strengths and dipole moments for the two molecules. The vertical absorption energy has been calculated at 4.47 and at 4.37 eV using MPW91-(Sm/Bg) and MPW91-Sm/B3LYP-Bg methods, respectively, in agreement with the experimental value of 4.18 eV measured in *n*-hexane. Contrary to TMAB-CN, which exhibits only a single band in the fluorescence spectra, NMC7 is dual fluorescent in a polar solvent like acetonitrile.[18] Similar compounds with five- and six-membered rings, such as 1-methyl-6-cyano-1,2,3,4-tetrahydroquinoline (NMC6) and 1-methyl-5-cyanoindoline (NMC5), do not exhibit dual fluorescence. These observations have been one of the origins of the planar ICT model put foward by Zachariasse et al.[2] According to this model, the N-inversion mode could not occur in NMC5 and NMC6 due to the rigidity of the cycle, whereas it does in NMC7 due to more flexibility. Those arguments are in line with the experimental facts that the former two molecules are not dual fluorescent, while the latter is.

Figure 9b displays the PES along the twisting coordinate, θ', of the ground and low-lying states of NMC7 computed using the MPW1PW91 functional. For each value of θ', a partial optimization of the seven-membered ring has been performed using the AM1 method. The ground and second excited states present a minimum for 60°. The charge-transfer excited state (1S) energy remains almost the same as θ' varies from 60 to 90°. For comparison, a partial optimization of the 7-ring at $\theta' = 90°$ using the MPW1PW91 functional has been performed. At this level of optimization, the twisted charge-transfer excited state with $\theta' = 90°$ is 0.10 eV more stable than the one corresponding to the optimized ground-state structure (i.e., $\theta' = 60°$). It can be noticed that the energy of all states increases as θ' varies from 60 to 0°. Our calculations are unable to reproduce the L_a emission measured at 2.66 eV in acetonitrile, because solvent effects are not treated explicitly. However, the
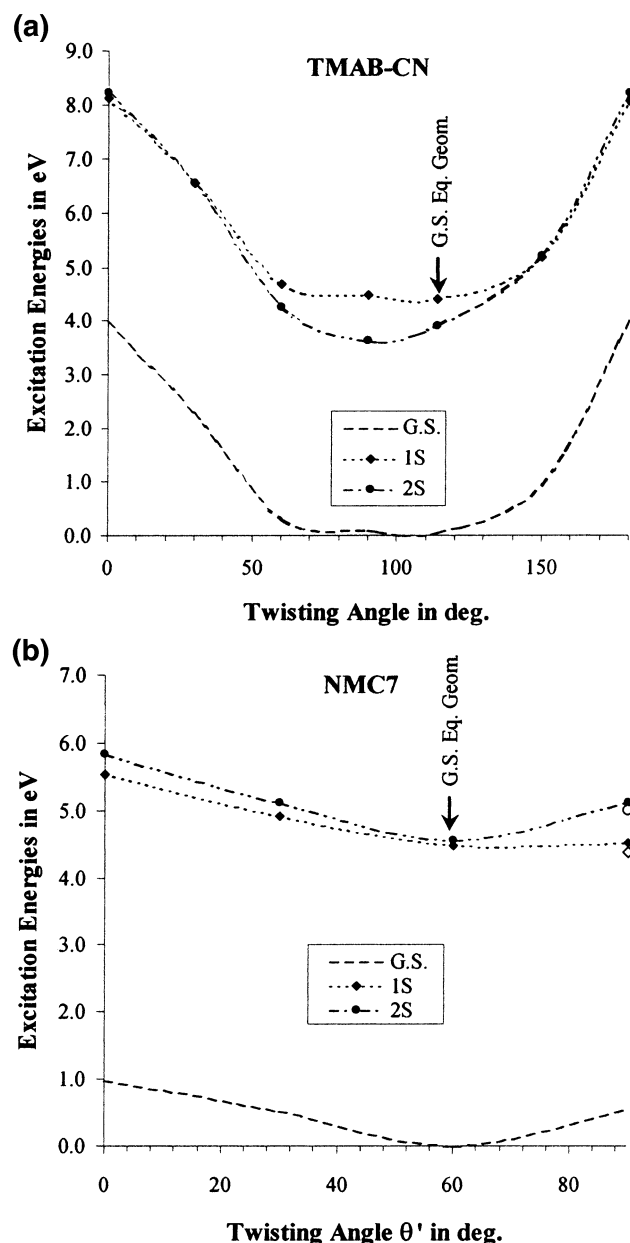
(a)

(b)

Figure 9. (a) PES along the twisting angle, θ, for TMAB-CN calculated using the B3LYP-(Sm/Bg) method. (b) PES along the twisting angle, θ' (see text), for the NMC7 molecule computed with the AM1/MPW91-Bg method. The empty symbols in the figure for $\theta = 90°$ represent calculations performed at the MPW91-(Sm/Bg) level.

potential energy surface provides a qualitative explanation of the fluorescence activity of this molecule. In polar solvents, the L_a band can be assigned to the charge-transfer excited state, whereas the L_b band could be attributed to an emission from the relaxed locally excited state. More profound investigations are needed for this molecule to obtain a quantitative answer.

C. The Potential Curves of 4DMAB-CHO and 4DMAB-NO₂. The optimization of geometry of 4DMAB-CHO leads to a planar structure. Experimental and calculated emission energies as well as their corresponding computed oscillator strengths and dipole moments are reported in Table 6. This molecule exhibits dual fluorescence only in polar solvents such as propanol or *n*-butyl chloride,[77] thus excluding direct comparison with our results. The potential energy surface of this molecule along the twisting angle is displayed in Figure 10a. As in the case of

Table 4. Experimental and Computed Singlet Excitation Energies (eV), Oscillator Strengths, *f*, and Dipole Moments, μ (D), for TMAB-CN Using Various Functionals (Emission Energies Have Been Computed at the Perpendicular Optimized Ground-State Geometry (TICT Model); the Reader Is Referred to Ref 65 for the Absorption Energies)

	G.S.[a]	1S → CT			2S → LE		
methods	μ	ΔE	f	μ	ΔE	f	μ
exp[75]		3.22					
exp[76]		3.22					
B3LYP-(Sm/Bg)[b,c]	5.84	3.56	0.00	21.06	4.40	0.00	18.93
MPW91-(Sm/Bg)[b,d]	5.85	3.72	0.00	20.63	4.58	0.00	18.76

[a] G.S. stands for ground state. [b] See Computational Section for more details about the notation used here. [c] For the ground state, an energy increase of 0.09 eV is calculated at $\theta = 90°$ as compared to the optimized ground state at $\theta = 114°$. [d] For the ground state, an energy increase of 0.11 eV is calculated at $\theta = 90°$ as compared to the optimized ground state at $\theta = 117°$.

4AB-CN, the potential energy surface of 4DMAB-CHO presents an avoided crossing along the twisting angle between the first and second excited states. The first vertical excited state, 1S, that corresponds to the transition from the lone pair on the oxygen, n_O, to the acceptor group, $\pi_{acceptor}$ (see Figure 3 for details about the molecular orbitals), will change nature along the twisting coordinate. This state will gain more charge-transfer character as the twisting angle increases, and, at $\theta = 90°$, it is mainly described by the transition from the lone pair on the nitrogen n_N to the acceptor group $\pi_{acceptor}$. The potential energy surface of this 1S state shows a minimum at $\theta = 90°$. Emission from the twisted 1S state is computed at 2.75 and 2.95 eV using the B3LYP and MPW1PW91 functionals, respectively. The dipole moment of the ground and second excited states decreases as the twisting angle increases, whereas the reverse variation is observed for the first excited state. An estimate of the energy barrier is computed at 0.26 eV using the MPW1PW91 functional.

For this molecule, the planar and wagging motions have also been investigated, but as in previous cases, no stabilization in energy has been computed for any state along the corresponding coordinates.

The 4DMAB-NO₂ molecule is structurally very similar to 4DMAB-CHO, both being planar systems. Table 7 displays experimental and calculated emission energies for this molecule as well as their corresponding computed oscillator strengths and dipole moments. Experimentally, this molecule is nondual fluorescent, and only a single band is observed in polar solvents. This has been attributed by Zachariasse et al.[18] to the presence of a large energy difference between the locally and charge-transfer excited states, supporting thus the planar ICT model where a small energy difference is necessary for both states to couple, to lead to a more stable structure. The potential energy surface of 4DMAB-NO₂ along the twisting angle is presented in Figure 10b. Unlike the 4DMAB-CHO case, it does not present any avoided crossing, and the lowest vertical excited state, 1S, keeps its charge-transfer character along the twisting coordinate, reaching an energy minimum for the perpendicular structure. The twisted charge-transfer excited state is more stable in energy

(75) Herbich, J.; Perez Salgado, F.; Rettschnick, R. P. H. *J. Phys. Chem.* **1991**, *95*, 3491.
(76) Rotkiewicz, K.; Rubaszewska, W. *J. Lumin.* **1982**, *27*, 221.
(77) Rettig, W.; Lutze, S. *Chem. Phys. Lett.* **2001**, *341*, 263.

Table 5. Experimental and Computed Singlet Excitation Energies (eV), Oscillator Strengths, *f*, and Dipole Moments, μ (D), for NMC7 Using Various Functionals (Absorption Energies Have Been Calculated at the Optimized Ground-State Geometry; for Emission Energies, a Partial Optimization of the Seven-Membered Ring Has Been Performed at the AM1 and MPW1PW91 Level, with $\theta' = 90°$)

| | absorption | | | | | | | emission | | | | | | |
| | G.S.[a] | 1S → CT | | | 2S → LE | | | G.S.[a] | 1S → CT | | | 2S → LE | | |
methods	μ	ΔE	f	μ	ΔE	f	μ	μ	ΔE	f	μ	ΔE	f	μ
exp[18]		4.18[b]							2.66[c]			3.48		
MPW91-(Sm/Bg)[d,e]	6.98	4.47	0.33	15.20	4.55	0.02	11.36	6.18	3.96	0.08	19.12	4.58	0.00	14.78
AM1/MPW91-Bg[d,f]								6.10	3.96	0.07	18.99	4.57	0.00	14.67
MPW91-Sm/B3LYP-Bg[d,g]	6.97	4.37	0.32	15.53	4.44	0.02	11.64	6.19	3.82	0.07	19.54	4.42	0.00	15.70

[a] G.S. stands for ground state. [b] Absorption and fluorescence spectra measured in *n*-hexane. [c] Fluorescence spectra measured in acetonitrile. [d] See Computational Section for more details about the notation used here. [e] For the ground state, an energy increase of 0.55 eV is calculated at $\theta' = 90°$ as compared to the optimized ground state at $\theta' = 60°$. [f] For the ground state, an energy increase of 0.41 eV is calculated at $\theta' = 90°$ using the AM1/MPW91-Bg method as compared to the optimized ground state computed at the MPW91-(Sm/Bg) level with $\theta' = 60°$. [g] For the ground state, an energy increase of 0.40 eV is calculated at $\theta' = 90°$ as compared to the optimized ground state at $\theta' = 60°$, using the MPW91-Sm/B3LYP-Bg method.

Table 6. Experimental and Computed Singlet Excitation Energies (eV), Oscillator Strengths, *f*, and Dipole Moments, μ (D), for 4DMAB-CHO Using Various Functionals (Emission Energies Have Been Computed at the Perpendicular Optimized Ground-State Geometry (TICT Model); Values in Parentheses Are Computed Using the MPW91(Sm/Bg) Method Otherwise Using the B3LYP-(Sm/Bg) Method; the Reader Is Referred to Ref 65 for the B3LYP Absorption Energies)

| | | emission | | |
state	nature of state	ΔE	f	μ
exp	CT	2.41[a]		
G.S.[b]		0.62		4.41
		(0.64)		(4.35)
1S	$n_N \rightarrow \pi_{acceptor}$	2.75	0.00	21.34
		(2.95)	(0.00)	(20.52)
2S	$n_O \rightarrow \pi_{acceptor}$	3.59	0.00	2.55
		(3.67)	(0.00)	(2.12)
3S	$n_N \rightarrow \pi^*_{phenyl}$	4.06	0.00	17.03
		(4.26)	(0.00)	(16.83)

[a] Measured in *n*-butyl chloride.[77] [b] G.S. stands for ground state. For the ground state, an energy increase of 0.62 and 0.64 eV is calculated at $\theta = 90°$ using the B3LYP-(Sm/Bg) and MPW91-(Sm/Bg) methods, respectively, as compared to the optimized ground state at $\theta = 0°$. The 1S, 2S, and 3S absorption energies have been computed at 3.86, 4.26, and 4.57 eV using the MPW91-(Sm/Bg) method.

than the planar conformer by 0.61 and 0.52 eV, and emission from this state is computed at 2.35 and 2.61 eV using B3LYP-(Sm/Bg) and MPW91-(Sm/Bg) methods, respectively. The nondual fluorescence of 4DMAB-NO$_2$ might be comparable to that of TMAB-CN. Again, the vertical charge-transfer excited state reaches, by a radiationless process, a perpendical structure, precursor of the L$_a$ emission. However, comparison between calculated and experimental emission energies for the L$_a$ band is difficult because the spectra have been recorded in polar solvents.[80,81] The computed dipole moments of the ground and second excited states decrease along the twisting path, whereas the reverse variation is observed for the first excited state with both functionals.

Both wagging and planar motions have been investigated showing no stabilization of the two lowest excited states. For both molecules, these models do not seem to apply.

IV. Discussion

Investigation of the mechanisms that are involved in the dual fluorescence is complex due to the interplay of dynamical, vibronic, electronic, and solvent effects. All of these parameters interact, modifying the potential energy surface and consequently the fluorescence emission. It is extremely complex to computationally model all of these interactions and to give a final answer to the physical-chemical mechanism involved in the process of the dual fluorescence. The solvent is probably one of the most important factors. Most experimental studies measure the L$_a$ band emission either in polar or in nonpolar solvents. The TMAB-CN molecule is the only case where gas-phase emission measurements have been performed. In our calculations, the solvent has not been treated, explicitly limiting the comparison between calculated and measured emission spectra. Another limiting parameter is the geometry of the excited state. Full optimization of geometry has been performed only for the ground electronic state structure, and the potential energy surface calculations are limited to the change of an angle or bond lengths, according to the investigated mechanism.

While the difference to the experimental results may be due to these shortcomings, results of this investigation still give insight into the mechanism of the dual fluorescence. For all molecules, it has been shown that the planar ICT model (investigated according to the coordinates of this work) does not lead to any energy stabilization for the charge-transfer excited state. The same observation is also valid for the wagging mechanism. According to our calculations, only the twisting ICT model appears to be a possible mechanism to explain the dual and nondual fluorescence. It is the only model that leads to an energy stabilization and to an increase of the dipole moment of the charge-transfer excited state along the twisting coordinate, reflecting the low energy and the strong solvent polarity dependence of the L$_a$ band.

As Rettig has mentioned in his papers, these donor−acceptor systems can be classified into two groups. The first, which includes 4DMAB-CN, 4AB-CN, and 4DMAB-CHO, corresponds to systems where the vertical charge-transfer excited state is above the locally excited state, which is the first excited state. For these systems, the nature of the first excited state changes along the twisting angle depending on the presence of an avoided crossing between the first and second excited states. If there is an avoided crossing, the first vertical excited state will

(78) Nicolet, P.; Laurence, C. *J. Chem. Soc., Perkin Trans. 2* **1986**, 1071.
(79) Laurence, C.; Nicolet, P.; Tawfik Dalati, M. *J. Phys. Chem.* **1994**, *98*, 8, 5807.
(80) Carsey, T. P.; Findley, G. L.; McGlynn, S. P. *J. Am. Chem. Soc.* **1979**, *101*, 4502.
(81) Schuddeboom, W.; Warman, J. M.; Biemans, H. A. M.; Meijer, E. W. *J. Chem. Phys.* **1996**, *100*, 12369.
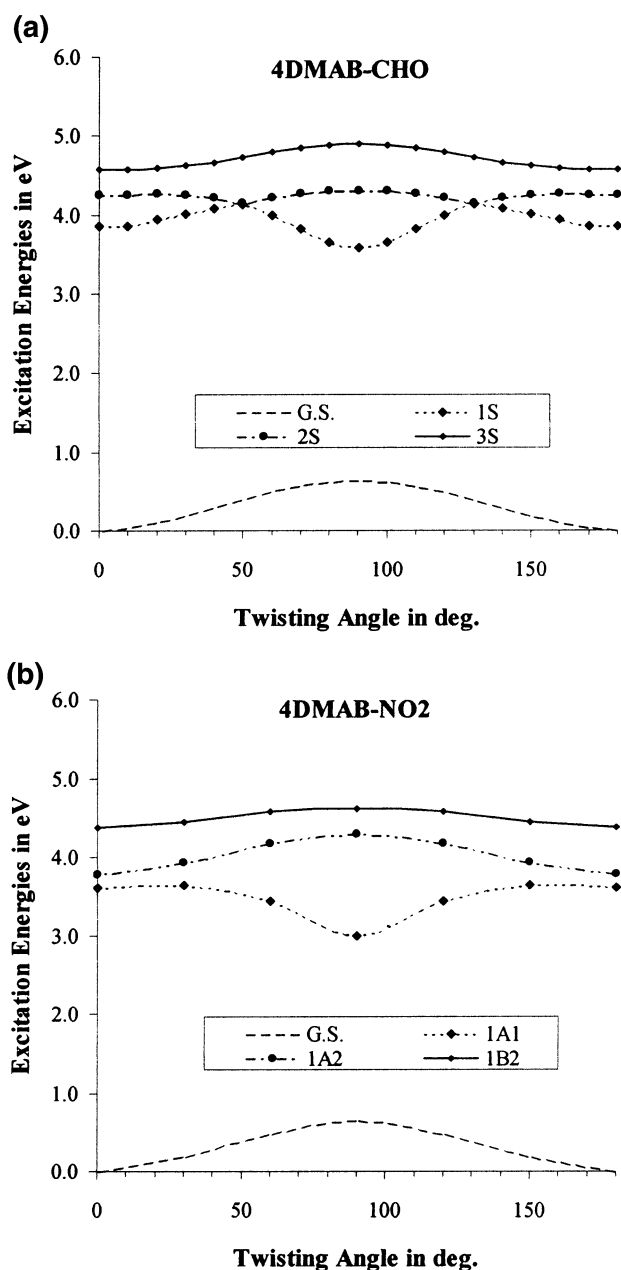
(a)

4DMAB-CHO

(b)

4DMAB-NO2

Figure 10. PES of the ground and low-lying singlet states for 4DMAB-CHO (a) and for 4DMAB-NO$_2$ (b) along the twisting coordinate calculated with the MPW91-(Sm/Bg) and B3LYP-(Sm/Bg) methods, respectively.

Table 7. Experimental and Computed Singlet Excitation Energies (eV), Oscillator Strengths, f, and Dipole Moments, μ (D), for 4DMAB-NO$_2$ Using Various Functionals (Emission Energies Have Been Computed at the Perpendicular Optimized Ground-State Geometry (TICT Model); Values in Parentheses Are Computed Using the MPW91-(Sm/Bg) Method Otherwise Using the B3LYP-(Sm/Bg) Method; the Reader Is Referred to Ref 65 for the B3LYP Absorption Energies)

		emission		
state	nature of state	ΔE	f	μ
exp	CT	2.81[a]		
		2.88[b]		
G.S.[c]		0.65		5.93
		(0.67)		(5.82)
1(^{1}A$_1$)	$n_N \rightarrow \pi_{acceptor}$	2.35	0.00	26.32
		(2.61)	(0.00)	(24.96)
1(^{1}A$_2$)	$n_O^- \rightarrow \pi_{acceptor}$	3.64	0.00	2.10
		(3.81)	(0.00)	(2.19)
1(^{1}B$_2$)	$n_N \rightarrow \pi_{benzene}^*$	3.97	0.00	18.67
		(4.18)	(0.00)	(18.41)
2(^{1}B$_2$)	$\pi_{phenyl} \rightarrow \pi_{acceptor}$	4.20	0.00	14.88
	($n_O^+ \rightarrow \pi_{acceptor}$)	(4.37)	(0.00)	(2.44)

[a] Measured in EPA solvent, see ref 80. [b] Measured in benzene solvent, see ref 81. [c] G.S. stands for ground state. For the ground state, an energy increase of 0.65 and 0.67 eV is calculated at $\theta = 90°$ using the B3LYP-(Sm/Bg) and MPW91-(Sm/Bg) methods, respectively, as compared to the optimized ground state at $\theta = 0°$. The 1(^{1}A$_1$), (^{1}A$_2$), (^{1}B$_1$), and (^{1}B$_2$) absorption energies have been computed at 3.80, 3.94, 4.50, and 4.52 eV using the MPW91-(Sm/Bg) method.

change nature from locally to charge transfer along this coordinate, and its energy profile will present an energy barrier whose highest value is related to the vertical energy gap between these two excited states. It is clear that the polarity of the solvent plays a role in modifying the vertical energy gap as well as the energy barrier, making the potential energy surface strongly dependent on the solvent nature. For these systems, the dual fluorescence is explained by a double mechanism within the twisting ICT model, already proposed by Serrano et al.[1] During the absorption, both the locally and the charge-transfer excited states are populated. The charge-transfer excited state will lose energy by a nonradiative process to the locally excited state from which the L$_b$ emission takes place. The locally excited state can also achieve a stabilization by following the hypersurface of the intramolecular twisting motion. From the final

perpendicular charge-transfer excited state, an emission occurs that is assigned to the L$_a$ band observed in the fluorescence spectra.

In the second group of molecules, 3DMAB-CN, TMAB-CN, and 4DMAB-NO$_2$, the first vertical excited state is the charge-transfer state. Here, the potential energy surface of the first excited state does not show an energy barrier because there is no avoided crossing. The energy of the vertical charge-transfer state decreases along the twisting angle, reaching an energy minimum for the perpendicular configuration. TMAB-CN is in that respect the most interesting example because gas-phase results exist, showing the prescence of only one band in the fluorescence spectra. This can be understood by the form of the potential energy surface of the first excited state that leads to an energy stabilization of the twisted charge-transfer state as compared to the vertical one. After absorption, the vertical charge-transfer state loses energy by a nonradiative process, reaching the twisted conformation from which the L$_a$ fluorescence occurs. 3DMAB-CN and 4DMAB-NO$_2$ are similar to TMAB-CN; they present only one band in the measured fluorescence spectra, and the calculated potential energy surface shows that the first vertical excited state is the charge-transfer state. According to our calculations, it seems likely that the vertical charge-transfer state of 4DMAB-NO$_2$ could reach a perpendicular structure because the gain in energy in twisting is equal to 0.61 and 0.52 eV using B3LYP-(Sm/Bg) and MPW91-(Sm/Bg) methods, respectively. However, this molecule is known to be nonfluorescent in nonpolar solvents. Instead, phosphorescence is observed, suggesting other patterns of deactivation. Fluorescence is only observed in polar solvents. In the case of 3DMAB-CN, the two functionals disagree in terms of the energy gain for the charge-transfer excited state along the twisting angle. The B3LYP-(Sm/Bg) method predicts an energy stabilization of 0.06 eV according to this coordinate, whereas a destabilization of 0.04 eV is computed using the

MPW91-(Sm/Bg) method. This case requires more investigations to reach a pertinent conclusion.

NMC7 belongs to the same group as TMAB-CN, where the first vertical excited state is the charge-transfer state. Therefore, this molecule is expected to show only one single band. The fluorescence spectra show only the locally band in *n*-hexane at 3.48 eV. However, in acetonitrile, both locally and charge-transfer bands are measured at 3.10 and 2.66 eV, respectively. Our calculations are unable to reproduce the charge-transfer energy measured in acetonitrile. However, from the potential energy surface, it can be seen that if an energy stabilization shall occur under solvent polarity, this will preferentially happen by twisting the angle to 90°. Here, it is interesting to notice the presence of a second excited state very close in energy to the vertical charge-transfer state (0.08 eV using B3LYP-(Sm/Bg)). In that case, the dual fluorescence might be explained also by a double mechanism. Both charge-transfer and locally excited states are populated in absorption. The locally excited state could relax by a nonradiative process to its energy minimum from which it emits (L_b band). The first charge-transfer excited state follows the adiabatic surface via intramolecular twisting motion, and emission occurs from the most stable twisted charge-transfer state (L_a band).

V. Conclusions

In this paper, TDDFT calculations have been performed for a set of dual (4DMAB-CN, 4DMAB-CHO, NMC7) and nondual (4AB-CN, 3DMAB-CN, TMABN, 4DMAB-NO$_2$) fluorescent molecules. For most of these systems, the PES according to the various mechanisms proposed in the literature, wagging, planar, and twisting ICT, have been investigated using B3LYP and/or MPW1PW91 functionals with a big (Bg) basis set. The geometry has been optimized for the ground electronic state structure using B3LYP or MPW1PW91 functionals with a small (Sm) basis set. For NMC7, partial geometry optimization of the 7-ring has been performed at the AM1 level for each twisting dihedral angle investigated.

For all molecules, the wagging ICT model, corresponding to the change of hybridization from sp^3 to sp^2 of the amino nitrogen, does not lead to a stabilization in energy of the charge-transfer excited state along the wagged coordinate.

No stable charge-transfer excited state having a quinoïdal structure has been found on the potential energy surface, which means that no support for the planar ICT model emerges from this study.

Within the twisting ICT model, a charge-transfer state having a twisted structure and a large dipole moment is predicted as a minimum on the potential energy surface being able to explain the presence of the strongly solvent-dependent L_a band, in the fluorescence spectra. Our calculations support the twisting ICT model as a possible mechanism to explain the dual fluorescence phenomenon. However, prediction about the occurrence of the dual fluorescence cannot be made only on the basis of structural arguments. More than the geometrical structure, the potential energy surface is of prime importance to make reliable predictions about the occurrence of this phenomenon. The predictiveness of the twisting ICT model requires complex calculations

of the potential energy surface that should ideally incorporate solvent effects.

In agreement with experimental data, 4AB-CN is calculated to be nondual fluorescent within the twisting ICT model. This is explained by the fact that the perpendicular 1S excited state is calculated higher in energy than its vertical conformer, preventing it from twisting.

TMAB-CN is single fluorescent in the gas phase, and this is nicely explained within the twisting ICT model. The molecule is already twisted in the ground-state geometry. From the perpendicular structure, the emission energy has been calculated at 3.56 eV using the B3LYP-(Sm/Bg) method, which has to be compared to the experimental value of 3.22 eV. One possible source of disagreement could be attributed to the geometry that has not been fully optimized for the twisted charge-transfer excited-state structure.

Like TMAB-CN, both 3DMAB-CN and 4DMAB-NO$_2$ present only one band in their fluorescence spectra, even in polar solvents. This could be understood looking at their potential energy surfaces, similar to that of TMAB-CN. The first excited state keeps its charge-transfer character along the twisting path, and no avoided crossing is observed. In the case of 4DMAB-NO$_2$, emission should occur from the twisted charge-transfer excited state. For 3DMAB-CN, more investigations are needed to clearly determine from which conformer (planar or twisted) the L_a emission takes place.

The 4DMAB-CN and 4DMAB-CHO molecules are similar in terms of their fluorescence spectra. The dual fluorescence is explained by the following double mechanism as already suggested by Serrano et al.[1] The L_b band is associated to the emission from the first vertical locally excited state, and the L_a band corresponds to the radiation from the twisted charge-transfer state that is reached by following the adiabatic surface according to the intramolecular twisting from the first vertical locally excited state. 4DMAB-CHO is dual fluorescent only in polar solvent, whereas 4DMAB-CN exhibits this phenomenon even in nonpolar solvent. This could be understood in terms of the energy barrier along the twisting angle that is higher in the case of 4DMAB-CHO than in 4DMAB-CN.

The dual fluorescence of NMC7 is nicely explained by the presence in the calculated absorption spectra of a locally excited state very close in energy from the first charge-transfer excited state. The L_b band corresponds to the emission from the locally excited state, whereas the L_a band results from the twisted charge-transfer state more stable in energy than the vertical conformer.

According to our calculations, only the twisting ICT model can explain the dual and nondual fluorescence of molecules investigated in this study.